

Hadron Correlations at Energies from GeV to TeV

W. KITTEL

Institute for Mathematics, Astrophysics and Particle Physics, Radboud
University Nijmegen/Nikhef, Nijmegen, Netherlands

Dedicated to Andrzej Bialas in honour of his 80th birthday

One of the central issues in High Energy Physics is the close interchange between Theory and Experiment. Ever since I know Andrzej Białas, I know him as one of the theorists most interested in experimental data. This has naturally led to continuous fruitful contacts.

Even though we have been working somehow together since about 1968, we so far have only one single publication in common. This was back in 1969 and it was on means to efficiently study what we then called (exclusive) Multihadron Final States. At that time this meant 3- or at best 4-particle final states of two-hadron collisions at cms energies of some 4 GeV (not TeV!). The field of multiparticle dynamics was in fact the domain of Polish high-energy physicists. The first of a very successful (and still lasting) series of annual International Symposia on Multiparticle Dynamics was organized in Paris in 1970, but essentially by Polish physicists. Andrzej himself was not attending, but it was he who organized the third in these series in (of course) Zakopane.

Since heavy-ion collisions, another field of major interest for Andrzej, will be covered by others, I here will restrict myself mainly to the collisions of two elementary particles.

PACS numbers: 12.38.Qk, 13.66.Bc, 13.85.Hd, 13.87.Fh

1. Exclusive longitudinal phase space analysis and its variables

One of our common interests at that time was the so-called Longitudinal Phase Space (LPS) Analysis of 3- and 4- or even 5-particle final states and I will first try to recall the ideas behind that.

The most complete way to study a so-called exclusive reaction of multiplicity n

$$A + B \longrightarrow C_1 + C_2 + \cdots + C_n \quad (1)$$

is to look at the differential distribution of its matrix element in full phase space. This, however, requires a $3n - 4$ dimensional analysis ($(3n - 5)$ -dimensional if the incident particles are unpolarized) and becomes increasingly impossible with increasing n .

Nature helps: at low cms energies, the vast majority of collisions is "soft", i.e. leads to low transverse (with respect to the collision axis) momenta of final state particles, largely independent of the nature of the particle, the multiplicity n and the cms energy $s^{1/2}$. On the other hand, longitudinal (along the collision axis) momenta are unlimited (i.e. limited only by phase space) and depend strongly on the nature of the particle, the multiplicity and the energy.

In elastic and other two-particle production collisions, one is used to distinguish between forward and backward scattering. An extension of this classification to multiparticle final states is an analysis in just longitudinal phase space (LPS) [1, 2]. Then, each individual reaction of type (1) is represented by a point with coordinates $(p_{\parallel 1}, \dots, p_{\parallel n})$ in a now only n -dimensional euclidean space S_n . Conservation of longitudinal momentum in the cms,

$$\sum_{i=1}^n p_{\parallel i}^* = 0, \quad (2)$$

defines LPS as an $(n-1)$ dimensional hyperplane L_{n-1} . Furthermore, because of conservation of cms energy $s^{1/2}$

$$\sum_{i=1}^n (m_i^2 + p_{\text{T}i}^2 + p_{\parallel i}^{*2})^{1/2} = s^{1/2}. \quad (3)$$

All points with equal transverse momentum $|p_{\text{T}i}|$ lie on an $(n-2)$ dimensional hypersurface K_{n-2} defined by (3). For the case of a transverse mass $m_{\text{T}i} = (m_i^2 + p_{\text{T}i}^2)^{1/2} = 0$, (3) reduces to

$$\sum_{i=1}^n |p_{\parallel i}^*| = s^{1/2} \quad (4)$$

and defines a regular polyhedron H_{n-2} . For $n = 3$, this is the Van Hove Hexagon shown in Fig. 1 together with the one-dimensional manifold K_1 . For $n = 4$, the polyhedron H_2 is the cuboctahedron celebrated in Fig. 2.

A typical three-particle distribution in LPS for the final state of reaction

$$\pi^- p \rightarrow p \pi^- \pi^0 \quad (5)$$

at an incident lab momentum of 16 GeV/c is given in Fig. 3 [3].

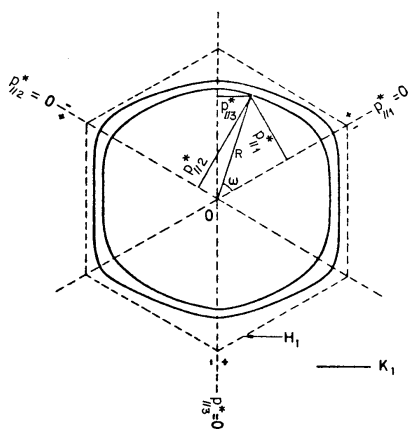


Fig.1. Longitudinal phase space plot (Van Hove Hexagon) for the final state $\pi\pi N$ at cms energy of $s^{1/2} = 4$ GeV. The innermost full line is K_1 for transverse momenta of 0.4, 0.4, and 0.5 GeV/c, respectively, while the outer one is K_1 for vanishing transverse momenta. The dashed line represents the hexagon H_1 [1].



Fig.2. The polyhedron H_2 for a four-particle final state (cartoon by R.Sosnowski).

The distribution of (5) against the angle ω is given in Fig. 4, before and after correcting for phase space effects (sub-figure (a) and (b), respectively). According to the definition in Fig. 1, the ω region considered ($60^\circ < \omega < 120^\circ$) corresponds to the hemisphere of LPS in which the proton is backward in the cms. The π^0 is taken to be longitudinally at "rest" at $\omega = 120^\circ$, the π^- at $\omega = 180^\circ$. Peaks in the (model-independent!) experimental data (histograms) indicate strong correlations between particles in the final state, in particular in the region $60 < \omega < 120^\circ$.

As a demonstration of how one can use LPS to test the success of theoretical models, the so-called CLA model [4] of that time was used. It is

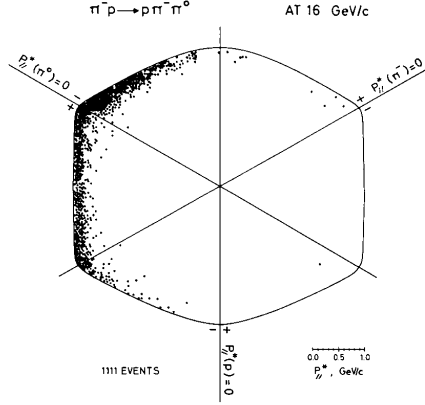


Fig. 3. Distribution of final state points for the reaction $\pi^- \rightarrow \pi^- \pi^0 p$ at incident lab momentum of 16 GeV/c [3].

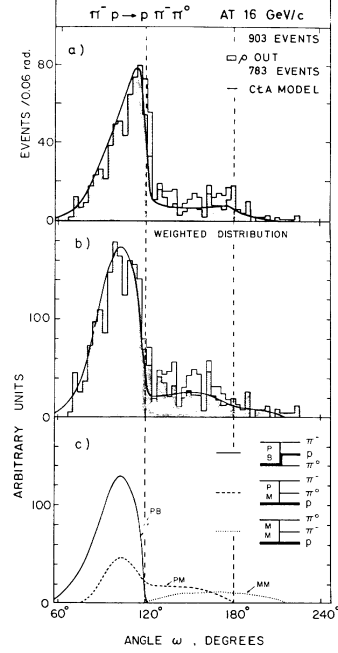


Fig. 4. (a) Distribution against the angle ω of final state points for the reaction $\pi^- p \rightarrow \pi^- \pi^0 p$ at incident lab momentum of 16 GeV/c [3]. (b) same after correcting for non-constant phase space effects. The solid lines are the distributions according to the CLA model [4] normalized to the data after exclusion of the sharp ρ^- -resonance. The individual CLA exchange graphs considered and their contributions to the total distribution are given in sub-figure (c).

a Reggeized form of a multiperipheral model, in which the amplitude is treated as an incoherent sum of contributions from various multiperipheral graphs. For the reaction studied in Fig. 4, they are given in sub-figure (c) together with their contributions. The full line in (a) and (b) corresponds to their incoherent sum. After exclusion of a sharp ρ -resonance, the model can describe the overall distribution of Fig. 4 surprisingly well. From the contribution of the graphs in sub-figure (c) we can see that vacuum exchange, commonly called IP(omeron) exchange, on the upper vertex essentially determines the shape of the distribution.

Turning back to a model independent data analysis, we investigate the energy dependence of the distribution and its shape in Fig. 5 according to its parametrization $\sigma(p_{\text{lab}}) \propto p_{\text{lab}}^{-N}$. As shown in sub-figure (b), N is indeed close to zero for $60^\circ < \omega < 120^\circ$, in agreement with IP exchange (diffraction

dissociation) in that region [5].

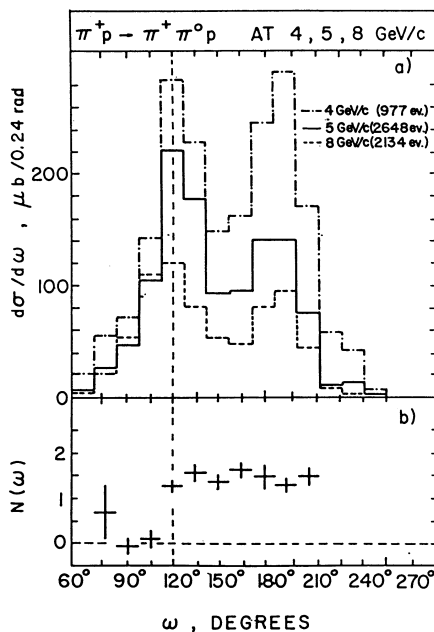


Fig. 5. (a) ω -distribution for the reaction $\pi^+p \rightarrow \pi^+\pi^0p$ at incident lab momentum of 4, 5 and 8 GeV/c. (b) Exponent N as a function of ω for the same reaction [5].

Where, however, is the Δ resonance? Unlike the incident proton, it has isospin $I = 3/2$ and can, therefore, not be produced via vacuum exchange.

One way to look for it, is the so-called prism plot [6] ingeniously combining the advantages of the angle ω along the z-axis with the subsystem masses given in a Fabri-Dalitz plot (triangle) at the basis (Figs. 6 and 7). The separation into individual mechanisms, each corresponding to a straight section of the tube within the prism, is better than in its projection onto the z-axis or the basis in the xy-plane. The mass of the $(p\pi^+)$ -subsystem is plotted in Fig. 8, for all events (sub-figure (a)) and for events in the corresponding section of the tube (sub-figure (b)). In the latter, the Δ^{++} is well separated from the background still present in (a).

Another way of extracting a pure Δ signal is a separation of the isospin matrix element according to the graph in Fig. 9. Since isospin exchange $I_E = 0$ is excluded for the production of the $I = 3/2$ ($N\pi$)-system, we are left with three matrix elements and their interferences. Their squares, respectively real parts, can readily be extracted model independently from combinations of the 6 measurable (of the 7 possible) final states of $\pi^\pm p$

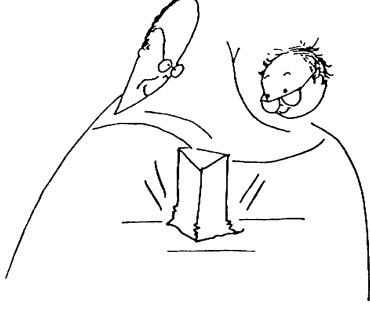


Fig. 6. The prism plot as constructed by pulling a Fabri-Dalitz plot out in the direction of the Van Hove angle ω (cartoon by Suzy Smile).

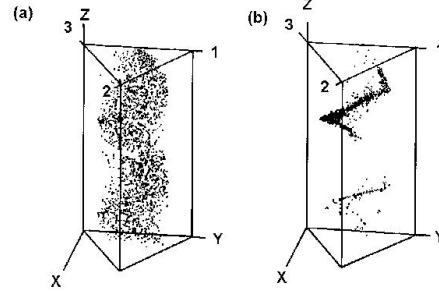


Fig. 7. Prism plot for $\pi^+p \rightarrow \pi^+\pi^0p$ at 3.9 GeV/c. (a) invariant phase space and (b) experimental data [6].

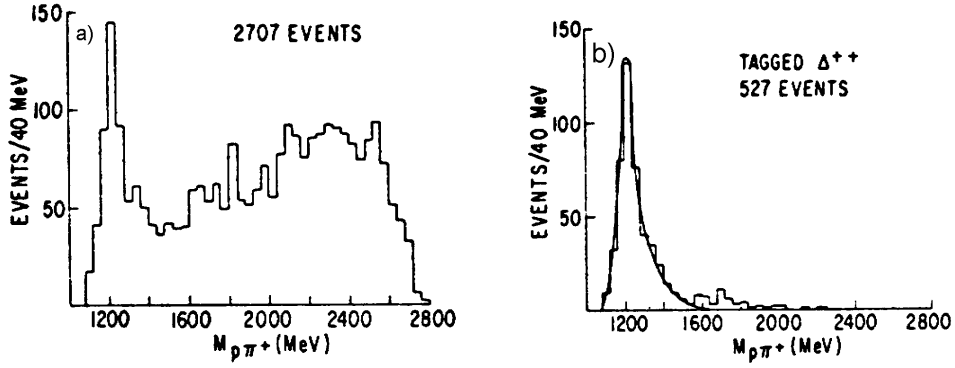


Fig. 8. Effective mass of the $(p\pi^+)$ -subsystem for the reaction $\pi^+p \rightarrow \pi^+\pi^0p$ at incident lab momentum of 3.9 GeV/c, for (a) all events and (b) for events in the corresponding section of the tube in the prism plot [6].

reactions. They are given in Fig. 10 as a function of the $(N\pi)$ effective mass. While a wide diffractive shoulder is observed in sub-figure (a), a sharp and well separated Δ can be seen in subfigure (c).

Overlap between different sub-systems is a problem, in particular in the determination of spin-parity of a particular sub-system (partial wave analysis). However, interference also provides a unique possibility to study the relative phase between overlapping amplitudes. In such a study, all mechanisms contributing to a particular few-body final state have to be treated simultaneously in an iterative and interactive computer analysis.

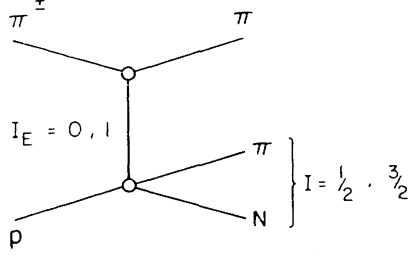


Fig. 9. The three diagrams corresponding to the amplitudes specified by the exchanged isospin I_E and the isospin I of the $(N\pi)$ system. (Note that the combination $I_E = 0, I = \frac{3}{2}$ is excluded from isospin conservation.)

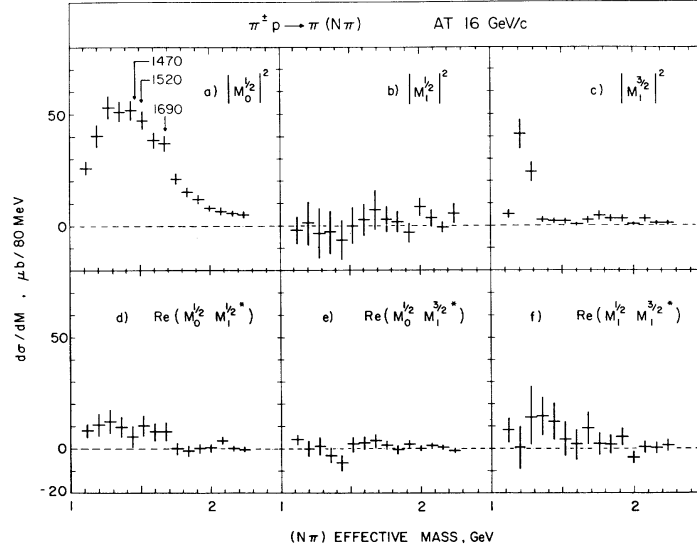


Fig. 10. Squared amplitudes $|M_I^{I_E}|^2$ and their interference terms as functions of the $(N\pi)$ mass obtained from the reactions $\pi^\pm p \rightarrow \pi\pi N$ at 16 GeV/c [7].

A beautiful method allowing that is the so-called Analytical Multichannel Analysis [8].

The method has successfully been applied to 30 000 events of the final state of $K^- p \rightarrow \bar{K}^0 \pi^- p$ at 4,2 GeV/c [9]. As the four variables needed to describe a three-particle final state, the effective mass M has been used for the sub-system considered, the invariant four-momentum t' in its production and the two angular variables Θ and ϕ of its decay.

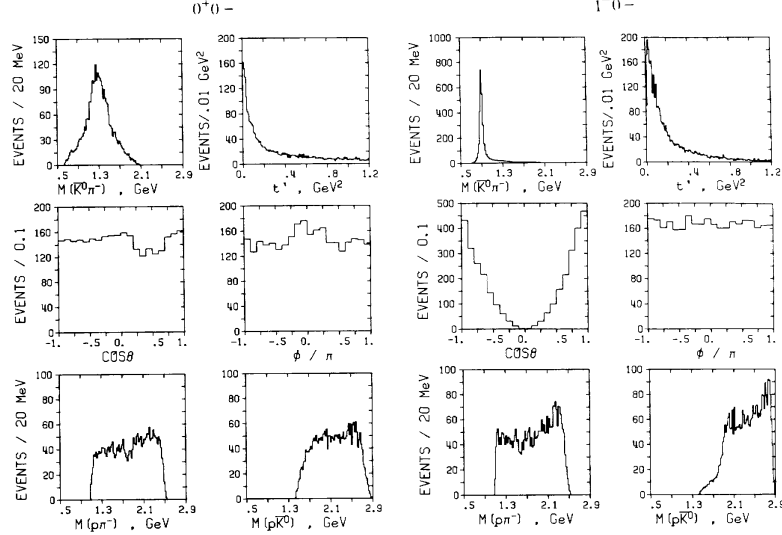


Fig. 11. Effective mass distribution of the $(\bar{K}^0 \pi^-)$ system, four-momentum transfer t' from initial to final state proton, decay angles of the $(\bar{K}^0 \pi^-)$ system, and effective mass of the $(p\pi^-)$ - and $(p\bar{K}^0)$ -systems for the 0^+0^- and 1^-0^- $(\bar{K}^0 \pi^-)$ samples after iteration 9 [9].

As examples for the results after 9 iterations, Figs. 11 and 12 correspond to the $(\bar{K}^0 \pi^-)$ S-wave and its P-waves 1^-0^- , 1^-1^- and 1^-1^+ . Except for the S-wave which is not yet flat, the angular distributions correspond to the particular wave and are as expected. Of particular interest are the differences in the four-momentum t' distributions for the three P-waves, typical for pseudo-scalar and vector exchange, respectively.

Striking is the difference in the reflection into the $(p\pi^-)$ and $(p\bar{K}^0)$ systems in the lowest row of Fig. 12. The Monte Carlo curve superimposed on the $(p\pi^-)$ mass distribution shows a two-peak reflection from the 1^-1^- wave. Just mind the enormous error introduced by the simple smooth hand-drawn background as used in earlier conventional analysis!

Very similar results are obtained [9] for the three D-and even F-waves and for other sub-channels down to the $\%$ level of their contribution to the total final state, not detectable in earlier analysis.

In conclusion from this section: With the help of model independent data analysis we have moved from analysis in Longitudinal Phase Space to a complete Multichannel Analysis. While the LPS analysis has demonstrated strong correlation of final state particles, the increased number of variables

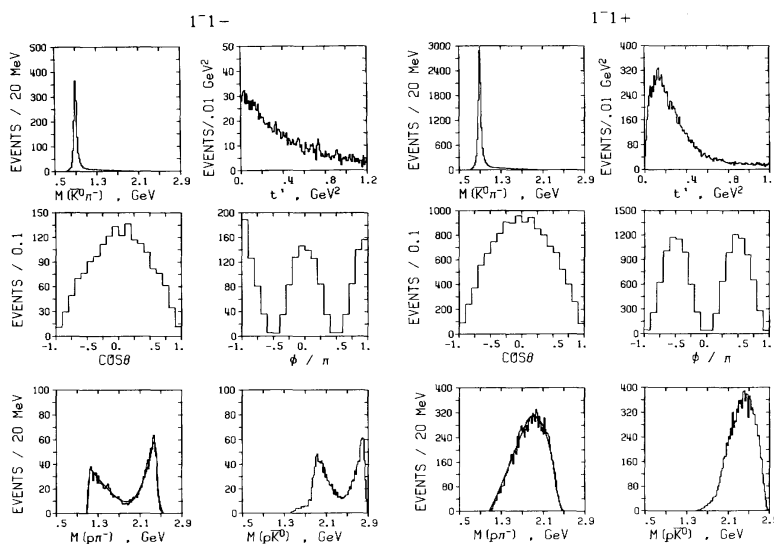


Fig. 12. Same as Fig. 11, but for the 1^-1^- and 1^-1^+ samples [9].

of the prism plot could show overlap of these mechanisms in full phase space (not just in projections of it). These mechanisms can be separated by means of quantum numbers as isospin, spin and angular momentum, and their interferences can be studied when all channels contributing to a final state are treated simultaneously. This analysis is particularly useful for the isolation of channels at the permille level of cross section or branching ratio.

What had we learned for the future? Experiments have to be *complete* in the sense that acceptance losses should be minimal and the four-vectors of all particles should be known. Furthermore, the analysis has to be done *iteratively and interactively*, i.e. has to be guided by computer graphics.

2. Momentum correlations and density fluctuations

2.1. The formalism

We start by defining symmetrized inclusive q -particle distributions

$$\rho_q(p_1, \dots, p_q) = \frac{1}{\sigma_{\text{tot}}} \frac{d\sigma_q(p_1, \dots, p_q)}{\prod_{i=1}^q dp_i}, \quad (6)$$

where $\sigma_q(p_1, \dots, p_q)$ is the inclusive cross section for q particles to be at p_1, \dots, p_q , irrespective of the presence and location of any further particles, p_i is the (four-) momentum of particle i and σ_{tot} is the total hadronic cross

section of the collision under study. For the case of identical particles, integration over an interval Ω in p -space yields

$$\begin{aligned} \int_{\Omega} \rho_1(p) dp &= \langle n \rangle , & \int_{\Omega} \int_{\Omega} \rho_2(p_1, p_2) dp_1 dp_2 &= \langle n(n-1) \rangle , \\ \int_{\Omega} dp_1 \dots \int_{\Omega} dp_q \rho_q(p_1, \dots, p_q) &= \langle n(n-1) \dots (n-q+1) \rangle , \end{aligned} \quad (7)$$

where n is the multiplicity of identical particles within Ω in a given event and the angular brackets imply the average over the event ensemble.

Besides the interparticle *correlations* we are looking for, the inclusive q -particle number densities $\rho_q(p_1, \dots, p_q)$ in general contain “trivial” contributions from lower-order densities. It is, therefore, advantageous to consider a new sequence of functions $C_q(p_1, \dots, p_q)$ as those statistical quantities which vanish whenever one of their arguments becomes statistically independent of the others [10, 11, 12]:

$$C_2(1, 2) = \rho_2(1, 2) - \rho_1(1)\rho_1(2) , \quad (8)$$

$$C_3(1, 2, 3) = \rho_3(1, 2, 3) - \sum_{(3)} \rho_1(1)\rho_2(2, 3) + 2\rho_1(1)\rho_1(2)\rho_1(3) , \quad (9)$$

etc. In the above relations, we have abbreviated $C_q(p_1, \dots, p_q)$ to $C_q(1, 2, \dots, q)$; the summations indicate that all possible permutations must be taken. Expressions for higher orders can be derived from the related formulae given in [13]. Deviations of these functions from zero shall be addressed as *genuine* correlations.

It is often convenient to divide the functions ρ_q and C_q by the product of q one-particle densities, which leads to the definition of the normalized inclusive densities and correlations:

$$R_q(p_1, \dots, p_q) = \rho_q(p_1, \dots, p_q) / \rho_1(p_1) \dots \rho_1(p_q), \quad (10)$$

$$K_q(p_1, \dots, p_q) = C_q(p_1, \dots, p_q) / \rho_1(p_1) \dots \rho_1(p_q). \quad (11)$$

In terms of these functions, correlations have been studied extensively for $q = 2$. Results also exist for $q = 3$, but usually the statistics (i.e. number of events available for analysis) are too small to isolate genuine correlations. To be able to do that for $q \geq 3$, one must apply factorial moments F_q defined via the integrals Eq. (7), but in limited phase-space cells [14, 15].

2.2. Density spikes

To see whether it is worth the effort, we first look for density fluctuations in single events, signalling high-order correlations. A notorious JACEE

event [16] (Fig. 13a) at a pseudo-rapidity resolution (binning) of $\delta\eta = 0.1$ has local fluctuations up to $dn/d\eta \approx 300$ with a signal-to-background ratio of about 1:1. An NA22 event [17] (Fig. 13b) contains a “spike” at a rapidity resolution $\delta y = 0.1$ of $dn/dy = 100$, as much as 60 times the average density in this experiment.

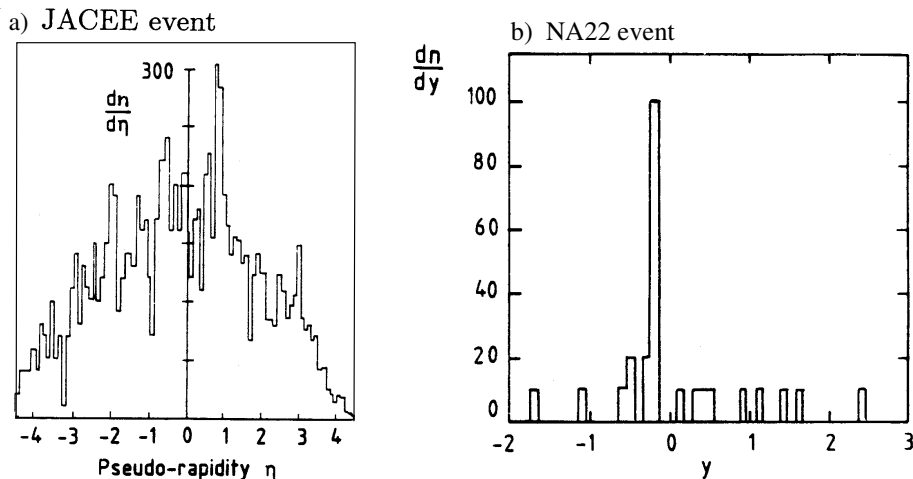


Fig. 13. a) The JACEE event [16]; b) The NA22 event [17].

Białas and Peschanski [14] suggested that this type of spikes could be a manifestation of “intermittency”, a phenomenon well known in fluid dynamics [18]. The authors argued that if intermittency indeed occurs in particle production, large density fluctuations are not only expected, but should also exhibit self-similarity with respect to the size of the phase-space volume.

In multiparticle experiments, the number of hadrons produced in a single collision is small and subject to considerable noise. To exploit the techniques employed in complex-system theory, a method had to be devised to separate fluctuations of purely statistical (Poisson) origin, due to finite particle numbers, from possibly self-similar dynamical fluctuations of the underlying particle densities. A solution, already used in quantum optics [19] and suggested for multiparticle production in [14], consists in measuring $F_q(\delta y)$ in given phase-space volumes (resolution) δy of ever decreasing size.

2.3. Power-law scaling

Besides the property of noise-suppression, high-order factorial moments act as a filter and resolve the large-multiplicity tail of the multiplicity distribution. They are thus particularly sensitive to large density fluctuations

at the various scales δy used in the analysis. As shown in [14], a smooth density distribution, which does not show any fluctuations except for the statistical ones, has the property of normalized factorial moments $F_q(\delta y)$ being independent of the resolution δy in the limit $\delta y \rightarrow 0$. On the other hand, if self-similar dynamical fluctuations exist, the F_q obey the power law

$$F_q(\delta y) \propto (\delta y)^{-\phi_q}, \quad (\delta y \rightarrow 0). \quad (12)$$

Equation (12) is a scaling law since the ratio of the factorial moments at resolutions L and ℓ

$$R = \frac{F_q(\ell)}{F_q(L)} = \left(\frac{L}{\ell} \right)^{\phi_q} \quad (13)$$

only depends on the ratio L/ℓ , but not on L and ℓ , themselves.

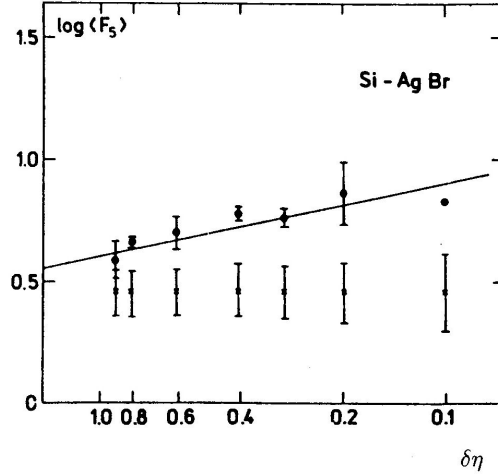


Fig.14. $\log F_5$ as a function of $-\log \delta \eta$ for the JACEE event [16] (full circles) compared to independent emission (small crosses) [14].

In Fig. 14, $\log F_5$ is plotted [14] as a function of $-\log \delta \eta$ (η is the pseudorapidity) for the JACEE event. It is compared with an independent-emission Monte-Carlo model tuned to reproduce the average η distribution of Fig. 13 a) and the global multiplicity distribution, but has no short-range correlations. While the Monte-Carlo model indeed predicts constant F_5 , the JACEE event shows a first indication for a linear increase, i.e. a possible sign of intermittency.

This observation was the trigger for a tremendous outburst of experimental research on all types of collisions from e^+e^- to heavy nuclei, all

showing (approximate) power law scaling. An 118 page summary including more than 300 references is given as chapters 7 and 10 in [20].

The powers ϕ_q (slopes in a double-log plot) are related [21] to the anomalous (or co-) dimensions $d_q = \phi_q/(q-1)$, a measure for the deviation from an integer dimension.

Anomalous dimensions d_q fitted over the (one-dimensional) range $0.1 < \delta y < 1.0$ are compiled in Fig. 15 [22]. They typically range from $d_q = 0.01$ to 0.1 , which means that the fractal (Rényi) dimensions $D_q = 1 - d_q$ are close to one. The d_q are larger and grow faster with increasing order q in μp and e^+e^- (Fig. 15a) than in hh collisions (Fig. 15b) and are small and almost independent of q in heavy-ion collisions (Fig. 15c). For hh collisions, the q -dependence is considerably stronger for NA22 ($\sqrt{s} = 22$ GeV, all p_T) than for UA1 ($\sqrt{s} = 630$ GeV, $p_T > 0.15$ GeV/c).

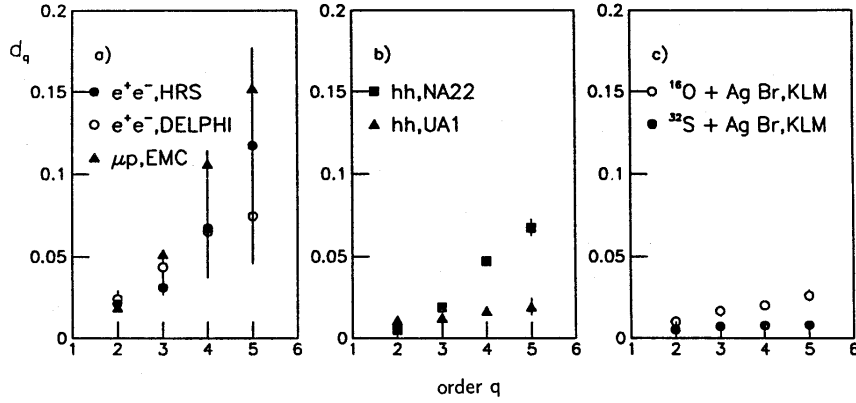


Fig. 15. Anomalous dimension d_q as a function of the order q , for a) μp and e^+e^- collisions, b) NA22 and UA1, c) KLM [22].

2.4. Factorial Cumulants

One further has to stress the advantages of normalized factorial cumulants K_q compared to factorial moments, since the former measure *genuine* correlation patterns.

As an example, high statistics data of the OPAL experiment [23] are given in Fig. 16 in terms of K_q , as a function of the number $M \propto 1/\delta y$ of phase space partitions for $q = 3$ to 5. In the leftmost column, the one-dimensional rapidity variable y is used for the analysis. The data (black dots) show an increase of K_q with increasing M for small M , but a saturation at larger M . Even though weaker, some saturation still persists

when the analysis is done in the two-dimensional plane of rapidity y and azimuthal angle φ (middle column), but approximate power-law scaling is indeed observed for the analysis in three-dimensional momentum space (right column). Thus, in high-energy collisions, fractal behavior is fully developed in three dimensions, while projection effects lead to saturation in lower dimension.

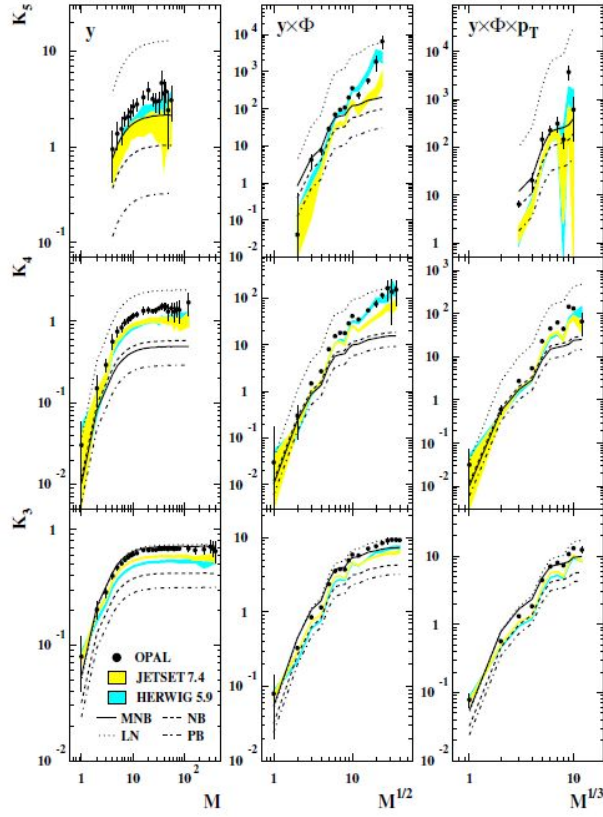


Fig. 16. Cumulants of order $q = 3$ to 5 as a function of $M^{1/D}$ in comparison with the predictions of various multiplicity parametrizations and two Monte Carlo models [23].

In Fig. 16, the data are also compared to a number of parametrizations of the multiplicity distributions, as well as to the Monte Carlo models JETSET and HERWIG. One can see that the fluctuations given by the negative binomial (NB) (dashed line) are weaker than observed in the data. Contrary to the NB, the log-normal (LN) distribution (dotted line) overestimates the

cumulants, while these expected for a pure birth (PB) process (dash-dotted) underestimate the data even more significantly than the NB. Among the distributions shown, a modified NB (MNB) gives the best results, even though significant underestimation is observed also there. The Monte Carlo models do surprisingly well.

2.5. Transverse-momentum dependence

An interesting question is whether semi-hard effects [24], observed to play a role in the transverse-momentum behavior even at NA22 energies [25], or low- p_T effects [26, 27] are at the origin of intermittency. A first indication for the latter comes from the most prominent NA22 spike event (Fig. 13b), where 5 out of 10 tracks in the spike have $p_T < 0.15$ GeV/ c .

In Fig. 17, NA22 data [28] on $\ln F_q$ versus $-\ln \delta y$ are given for particles with transverse momentum p_T below and above 0.15 GeV/ c , and with p_T below and above 0.3 GeV/ c . For particles with p_T below the cut (left), the F_q exhibit a far stronger δy dependence than for particles with p_T above the cut (right).

UA1 has a bias against $p_T < 0.15$ GeV/ c and the anomalous dimension is indeed smaller in UA1 than in NA22 in Fig. 15. We conclude that intermittency in hh collisions is not dominated by semi-hard effects.

2.6. Energy and multiplicity dependence

As seen in Fig. 18, a strong multiplicity dependence of the intermittency strength is observed for hh collisions by UA1 [29]. The trend is opposite to the predictions of the models used by this collaboration. This decrease of the intermittency strength with increasing multiplicity is usually explained as a consequence of mixing of independent sources of particles [21].

Mixing of emission sources leads to a roughly linear decrease of the slopes ϕ_q with increasing particle density $\langle \rho \rangle$ in rapidity [30, 31, 32]: $\phi_q \propto \langle \rho \rangle^{-1}$. This is indeed observed by UA1 [29].

Fig. 18a helps in explaining why intermittency is so weak in heavy-ion collisions (cfr. Fig. 15): the density (and mixing of sources) is particularly high there. In Fig. 18b, EMU01 [33], therefore, compares ϕ_2 for NA22 (hp at 250 GeV) and heavy-ion collisions at similar beam momentum per nucleon, as a function of the particle density. Whereas slopes averaged over multiplicity are smaller for AA collisions than for NA22 in Fig. 15, at fixed $\langle \rho \rangle$ they are actually higher than expected from an extrapolation of hh collisions to high density and may even grow with increasing size of the nuclei. The trend is confirmed by KLMM [34] for intermittency in azimuthal angle φ and for slopes up to order 5. This may be evidence for re-scattering (see [35]) or another (collective) effect, but, as shown by HELIOS [36] and

confirmed by EMU-01 [33], one has to be very sure about the exclusion of γ -conversions before drawing definite conclusions.

2.7. Density and correlation integrals

A fruitful development in the study of density fluctuations is the density and correlation strip-integral method [37] illustrated in Fig. 19 [38]. By means of integrals of the inclusive density over a strip domain in y_1, y_2 space, rather than a sum of box domains, one not only avoids unwanted side-effects such as splitting of density spikes, but also drastically increases the integration volume (and therefore the statistical significance) at given resolution. In terms of the strips (or hyper-tubes for $q > 2$), the density integrals can be evaluated directly from the data after selection of a proper distance measure, as e.g. the four-momentum difference $Q_{ij}^2 = -(p_i - p_j)^2$, and after definition of a proper multiparticle topology (snake integral [39], GHP integral [37], star integral [40]). Similarly, *correlation* integrals can be defined by replacing the density ρ_q in the integral by the correlation function

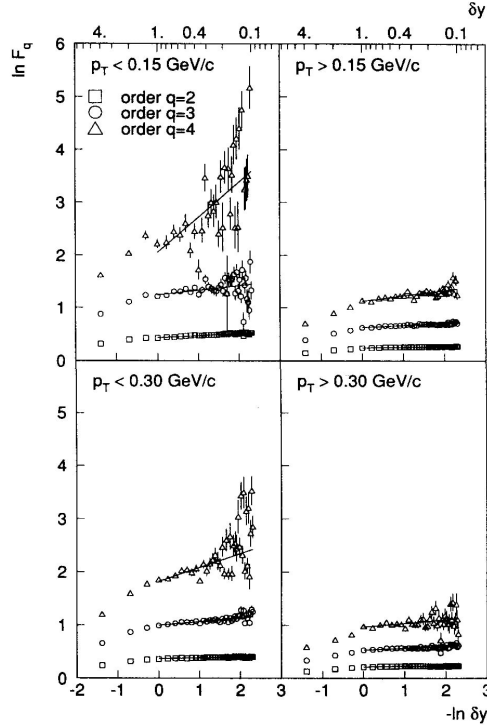


Fig. 17. $\ln F_q$ as a function of $-\ln \delta y$ for various p_T cuts as indicated [28].

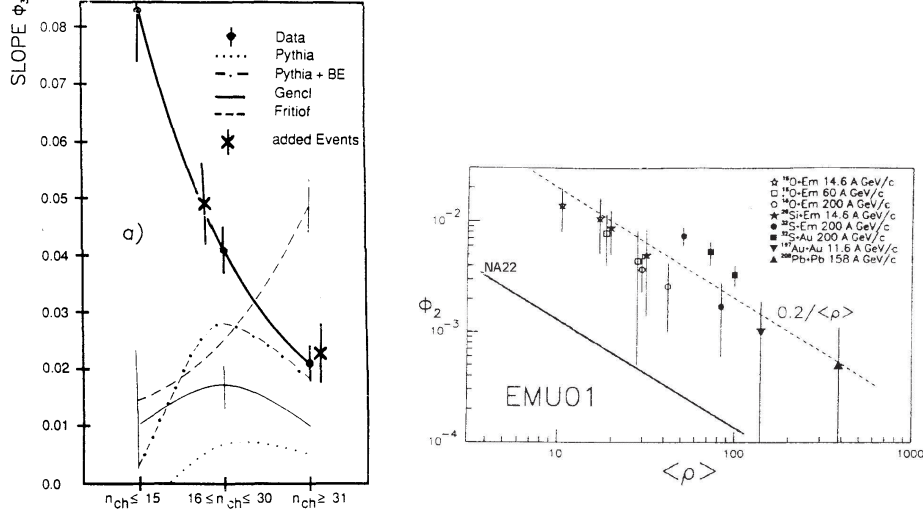


Fig. 18. a) Multiplicity dependence of the slope ϕ_3 , compared to that expected from a number of models, the crosses correspond to a combination of independent events [29], b) slope ϕ_2 extrapolated ($\propto \rho^{-1}$) as a function of particle density from NA22 (hp at 250 GeV) (solid line) and heavy-ion collisions as indicated [33].

C_q .

Of particular interest is a comparison of hadron-hadron to e^+e^- results in terms of same and opposite charges of the particles involved. Such a comparison is shown in Fig. 20 for $q = 2$ [41]. An important difference between UA1 and DELPHI can be observed in a comparison of the two sub-figures: For relatively large $Q^2 (> 0.03 \text{ GeV}^2)$, where Bose-Einstein effects do not play a major role, the e^+e^- data increase much faster with increasing $-\log Q^2$ than the hadron-hadron results. For e^+e^- , the increase in this Q^2 region is very similar for same and for opposite-sign charges. At small Q^2 , however, the e^+e^- results approach the hh results. For e^+e^- annihilation at LEP at least two processes are considered to be responsible for the power-law behavior: Bose-Einstein correlation at small Q^2 following the evolution of jets at larger Q^2 , but what is remarkable is the smooth transition between the two domains (if at all present) (see Sect. 3).

2.8. Genuine higher-order correlations

The correlation integral method turns out particularly useful for the unambiguous establishment of genuine higher-order correlations in terms of the normalized cumulants $K_q(Q^2)$, when using the star integration [40].

Non-zero values of (star integral) $K_q^*(Q^2)$ increasing according to a power law with decreasing Q^2 were first observed in NA22 up to fifth order [42] (see Fig. 21) and in E665 for third order [43]. Again note the difference between all charged and like charged particles and the smooth transition between larger and smaller Q^2 .

2.9. Functional form

The exact functional form of F_2^S is derived from the data of UA1 [29] and NA22 [38]¹ in Fig. 22. Clearly, the data favour a power law in Q over an exponential, double-exponential or Gaussian law.

If the observed effect is real, it supports a view developed in [44]. There, intermittency is explained from Bose-Einstein correlations between (like-charged) pions. As such, Bose-Einstein correlations from a static source are not power behaved. A power law is obtained i) if the size of the interaction region is allowed to fluctuate, and/or ii) if the interaction region itself is assumed to be a self-similar object extending over a large volume. Condition ii) would be realized if parton avalanches were to arrange themselves into self-organized critical states [45]. Though quite speculative at this moment, it is an interesting new idea with possibly far-reaching implications. We

¹ In fact in this form $F_2^S(Q^2)$ is identical to $R(Q^2)$ usually used in Bose-Einstein analysis. The only difference is that it is plotted on a double-logarithmic plot, here.

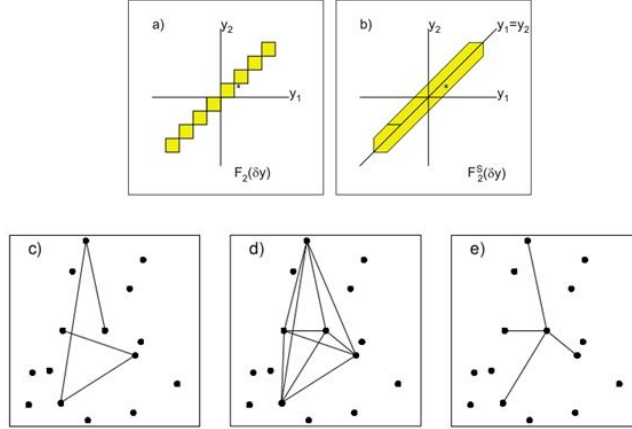


Fig. 19. a) The integration domain $\Omega_B = \Sigma_m \Omega_m$ of $\rho_2(y_1, y_2)$ for the bin-averaged factorial moments, b) the corresponding integration domain Ω_S for the density integral, c) illustration of a q -tuple in snake topology, d) GHP topology, e) star topology [38].

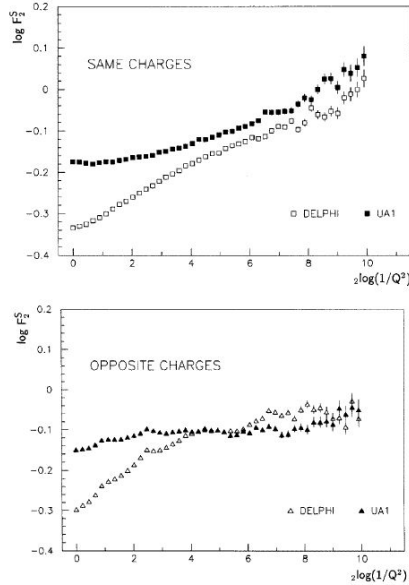


Fig. 20. Comparison of density integrals for $q = 2$ in their differential form (in intervals Q^2, Q^2+dQ^2) as a function of $2 \log(1/Q^2)$ for e^+e^- (DELPHI) and hadron-hadron collisions (UA1).[41]

should mention also that in such a scheme intermittency is viewed as a final-state effect and is, therefore, not troubled by hadronization effects.

So, in conclusion of this section, (approximate) intermittency is found to be all-present in hadron production and is evidence for genuine correlations to high orders, but it seems dominated by Bose-Einstein correlations. However, what we have learned is that we have been fooled for more than half a century by an assumed Gaussian behavior of the BE correlations, while an approximate power law is required. This highly non-trivial lesson we have learned indeed throws a completely new light on the topic of femtoscopy.

3. Bose-Einstein Correlations (or what?)

3.1. Early results

Whether derived as Fourier transform of a (static and chaotic) pion source distribution, a covariant Wigner-transform of the (momentum dependent) source density matrix, or from the string model, identical-pion correlation leads to a positive, non-zero two-particle correlator $K_2(Q)$, i.e.

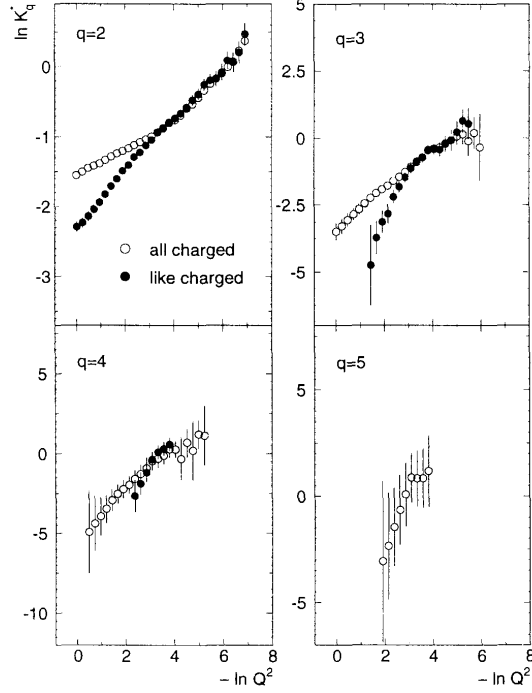


Fig. 21. $\ln K_q^*(Q^2)$ as a function of $-\ln Q^2$ for all charged particles as well as for like-charged particles [42].

to

$$R_2(Q) = 1 + K_2(Q) > 1 \quad (14)$$

at small four-momentum difference Q . These so-called Bose-Einstein Correlations, by now, are a well-established effect in all types of collisions, even in hadronic Z^0 decay (for reviews see [20, 46, 47]) originally expected, however, to be too coherent to show an effect.

Other important observations are given in abstract form below.

1. When evaluated in two (or better three) dimensions in the Bertsch-Pratt system, a small elongation of the emission region (better region of homogeneity [48] is observed along the event axis in all types of collisions (hadron-hadron [49], all four LEP experiments [50], ZEUS [51], RHIC [52]). However, it is important to note that the longitudinal radius of homogeneity is much shorter than the length of the string (of order 1%).

The observation that the out-radius does not grow beyond the side-radius at RHIC [52] points to a short duration of emission and causes a problem for some hydrodynamical models, but not for e.g. the Buda-Lund

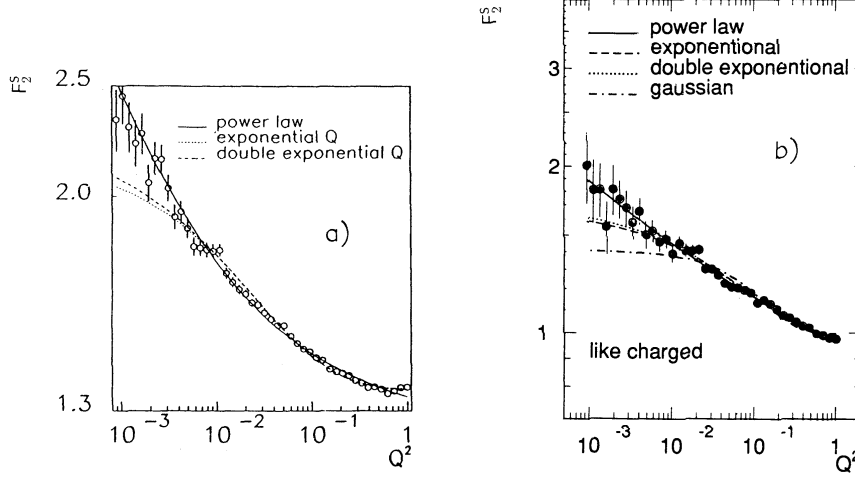


Fig. 22. Density integrals F_2^S (in their differential form) as a function of Q^2 for like-charged pairs in UA1 [29] and NA22 [38], compared to power-law, exponential, double-exponential and Gaussian fits, as indicated.

hydro model. The latter, in fact gives a beautifully consistent description of single-particle spectra and BEC in hadron-hadron and heavy-ion collisions at SPS and RHIC [53]. The emission function resembles a Gaussian shaped fire-ball for AA collisions, but a fire-tube for hh collisions.

2. The form of the correlator at small Q is steeper than Gaussian, in fact consistent with a power law as would be expected from the intermittency phenomenon described above. Unifying progress is reported in [54].

3. An approximate $m_T^{-1/2}$ scaling first observed in heavy-ion collisions at the SPS [55] and usually blamed on collective flow, is observed at RHIC [56], but also in e^+e^- collisions [57]. Quite generally, it follows from a strong position momentum correlation [58], be it due to collective flow or to string fragmentation.

4. *Genuine three-pion correlations* exist in all types of collisions and, in principle, allow a phase to be extracted from

$$\cos \phi \equiv \omega(Q_3) = K_3(Q_3)/2\sqrt{K_2(Q_3)}. \quad (15)$$

At small Q , this ω is near unity (as expected from incoherence) for hh [59] and e^+e^- [60] collisions, as well as for PbPb [61, 62] and AuAu [63] collisions at SPS and RHIC, while it is near zero (compatible with full coherence) in collisions of light nuclei [61]. This contradiction can be solved [46, 64] if ω is interpreted as a ratio of normalized cumulants. Since $K_q^{(N)}$

of N independent overlapping sources gets diluted like $1/N^{q-1}$, ω would be reduced if strings produced by light ions do not interact. If, in *heavy* ion collisions, the string density gets high enough for them to coalesce, some kind of percolation sets in and full inter-string BEC gets restored.

5. Azimuthal anisotropy is observed in configuration space of non-central heavy-ion collisions at AGS energies [65], but also at RHIC [66]. Contrary to elliptic flow, it is directed out of the event plane, but consistent with the elliptic nuclear overlap in a non-central collision. Due to larger pressure in the event plane, the anisotropy gets reduced but not destroyed at RHIC. Also this is evidence for a short duration of pion emission.

3.2. The τ model

In e^+e^- , BEC depend, at least approximately, only on Q and not on its components separately, in the sense that e^+e^- BEC is large if Q is small even when any of its components are large. Further, R_2 shows anti-correlations in the region 0.6–1.5 GeV as observed by L3 at LEP [67] as well as by CMS [68] and ATLAS (preliminary) [69] at LHC (see Fig. 23).

A model which predicts such Q -dependence, as well as the absence of dependence on the components of Q separately, is the so-called τ -model [70]. Further it incorporates the Bjorken-Gottfried condition [71] whereby the four-momentum of a produced particle and the space-time position at which it is produced are linearly related.

In this model, it is assumed that the average production point in the overall center-of-mass system, $\bar{x} = (\bar{t}, \bar{r}_x, \bar{r}_y, \bar{r}_z)$, of particles with a given four-momentum $p = (E, p_x, p_y, p_z)$ is given by

$$\bar{x}^\mu(p^\mu) = a\tau p^\mu. \quad (16)$$

In the case of two-jet events, $a = 1/m_T$ where m_T is the transverse mass and $\tau = \sqrt{\bar{t}^2 - \bar{r}_z^2}$ is the longitudinal proper time. For isotropically distributed particle production, the transverse mass is replaced by the mass in the definition of a and τ is the proper time, $\sqrt{\bar{t}^2 - \bar{r}_x^2 - \bar{r}_y^2 - \bar{r}_z^2}$.

The second assumption is that the distribution of $x^\mu(p^\mu)$ about its average, $\delta_\Delta(x^\mu(p^\mu) - \bar{x}^\mu(p^\mu))$, is narrower than the proper-time distribution, $H(\tau)$. Then the two-particle Bose-Einstein correlation function is indeed found to depend on the invariant relative momentum Q , rather than on its separate components, as well as on the values of a of the two particles [72]:

$$R_2(p_1, p_2) = 1 + \text{Re} \tilde{H} \left(\frac{a_1 Q^2}{2} \right) \tilde{H} \left(\frac{a_2 Q^2}{2} \right), \quad (17)$$

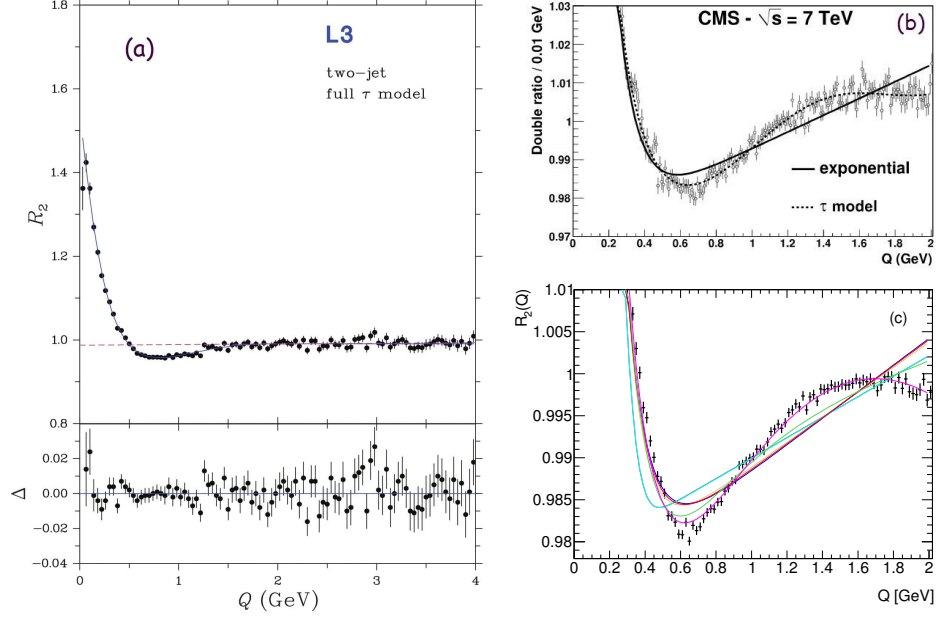


Fig. 23. The Bose-Einstein correlation function R_2 for a) L3 [67], b) CMS [68] and c) ATLAS [69]. The curve in (a), the dashed line in (b) and the best fit in (c) correspond to the fit of the τ model. The results of the L3 fit are given in Table 1. Also plotted in (a) is Δ , the difference between the fit and the data. The dashed line represents the long-range part of the fit, i.e., $\gamma(1 + \epsilon Q)$. The full line in (b) is an exponential fit. The lines in (c) correspond to Gaussian, exponential, and τ model fits.

where $\tilde{H}(\omega) = \int d\tau H(\tau) \exp(i\omega\tau)$ is the Fourier transform (characteristic function) of $H(\tau)$. (Note that $H(\tau)$ is normalized to unity.)

Since there is no particle production before the onset of the collision, $H(\tau)$ should be a one-sided distribution. In the leading log approximation of QCD the parton shower is a fractal [73]. Further, a Lévy distribution arises naturally from a fractal [74]. One is thus led to choose a one-sided Lévy distribution for $H(\tau)$ [72]. The characteristic function of $H(\tau)$ can then be written [75] (for $\alpha \neq 1$) as

$$\tilde{H}(\omega) = \exp \left[-\frac{1}{2} (\Delta\tau|\omega|)^\alpha \left(1 - i \operatorname{sign}(\omega) \tan \left(\frac{\alpha\pi}{2} \right) \right) + i\omega\tau_0 \right], \quad (18)$$

where the parameter τ_0 is the proper time of the onset of particle production and $\Delta\tau$ is a measure of the width of the proper-time distribution. $0 < \alpha < 2$

is the so-called index of stability [76] of the Lévy distribution. Using this characteristic function in (17), and incorporating the usual strength factor λ and the long-range parametrization, yields

$$R_2(Q, a_1, a_2) = \gamma \left\{ 1 + \lambda \cos \left[\frac{\tau_0 Q^2 (a_1 + a_2)}{2} + \tan \left(\frac{\alpha \pi}{2} \right) \left(\frac{\Delta \tau Q^2}{2} \right)^\alpha \frac{a_1^\alpha + a_2^\alpha}{2} \right] \right. \\ \left. \cdot \exp \left[- \left(\frac{\Delta \tau Q^2}{2} \right)^\alpha \frac{a_1^\alpha + a_2^\alpha}{2} \right] \right\} (1 + \epsilon Q) . \quad (19)$$

It is the cosine factor which generates oscillations corresponding to alternating correlated and anti-correlated regions mentioned above. Note also that since $a = 1/m_T$ for two-jet events, the τ -model predicts a decrease of the effective source size with increasing m_T .

Table 1. Results of the fit of (19) for two-jet events, as shown in Fig. 23 a) [67]. The parameter τ_0 is fixed to zero. The first uncertainty is statistical, the second systematic.

parameter	
λ	$0.58 \pm 0.03^{+0.08}_{-0.24}$
α	$0.47 \pm 0.01^{+0.04}_{-0.02}$
$\Delta \tau$ (fm)	$1.56 \pm 0.12^{+0.32}_{-0.45}$
ϵ (GeV $^{-2}$)	$0.001 \pm 0.001 \pm 0.003$
γ	$0.988 \pm 0.002^{+0.006}_{-0.002}$
χ^2/DoF	90/95
confidence level	62%

For each bin in Q the average values of m_{T1} and m_{T2} are calculated, where m_{T1} and m_{T2} are the transverse masses of the two particles making up a pair, requiring $m_{T1} > m_{T2}$. Using these averages, (19) is fit to $R_2(Q)$ by the L3 Coll. [67]. The fit results in $\tau_0 = 0.00 \pm 0.02$ fm, and the results of a re-fit with τ_0 fixed to zero are shown in Table 1.

Note that no significant long-range correlation is observed: $\epsilon = 0$ well within one standard deviation and γ is close to unity. Obviously, the τ -model by itself can reproduce the (smooth) shape of the Q -distribution over the full range considered, the anticorrelation near $Q=0.6$ GeV included.

In the τ -model, the basic assumption is the Bjorken-Gottfried condition [71] leading to (16). Recently, it has been demonstrated by the same authors [77], however, that already the compositeness of pions can most naturally

lead to an anti-correlation. At small distances the constituents mix and there are no separate pions to interfere.

3.3. The emission function

The τ model results for BEC can be used together with the single-particle inclusive spectra to reconstruct the space-time evolution of hadronization. The emission function in configuration space, $S_x(x)$, is the proper time derivative of the integral over p of $S(x, p)$ [72]. Approximating δ_Δ by a Dirac delta function again, gives

$$S_x(x) = \frac{1}{\bar{n}} \frac{d^4 n}{d\tau d^3 x} = \left(\frac{m_T}{\tau} \right)^3 H(\tau) \rho_1 \left(p = \frac{m_T x}{\tau} \right), \quad (20)$$

where n and \bar{n} are the number and average number of pions produced, respectively, and $\rho_1(p)$ is the experimentally measurable single-particle spectrum.

Given the symmetry of two-jet events, S_x does not depend on the azimuthal angle, and one can write it in cylindrical coordinates as

$$S_x(r, z, t) = P(r, \eta) H(\tau), \quad (21)$$

where η is the space-time rapidity. With the strongly correlated phase-space of the τ -model, η is equal to the momentum-energy rapidity y and $r = p_T \tau / m_T$. Consequently,

$$P(r, \eta) = \left(\frac{m_T}{\tau} \right)^3 \rho_{p_T, y}(r m_T / \tau, \eta), \quad (22)$$

where $\rho_{p_T, y}$ is the joint single-particle distribution of p_T and y .

The reconstruction of S_x is simplified if $\rho_{p_T, y}$ can be factorized into the product of the single-particle p_T and rapidity distributions, *i.e.*, $\rho_{p_T, y} = \rho_{p_T}(p_T) \rho_y(y)$. Then (22) becomes

$$P(r, \eta) = \left(\frac{m_T}{\tau} \right)^3 \rho_{p_T}(r m_T / \tau) \rho_y(\eta), \quad (23)$$

The integral over the transverse distribution is shown in Fig. 24. It exhibits a "boomerang" shape with a maximum at low t and z , but with tails reaching out to very large values of t and z , a feature already observed for hadron-hadron [78, 79] and heavy ion collisions [80] (Fig. 25 a) and c)) in the framework of a hydrodynamical model [81].

The transverse part of the emission function is obtained by integrating over z as well as azimuthal angle. Fig. 26 shows the transverse part of the

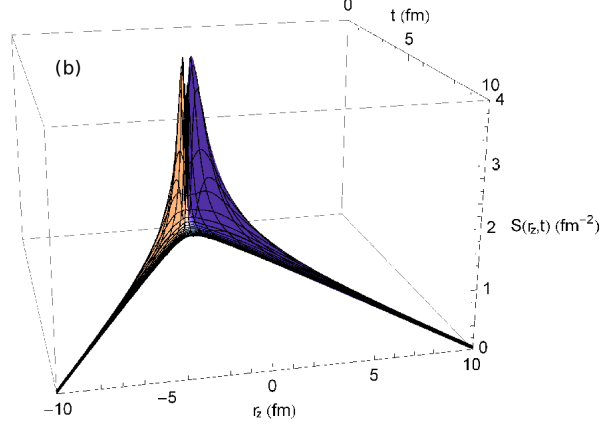


Fig. 24. The temporal-longitudinal part of the emission function normalized to unity [67].

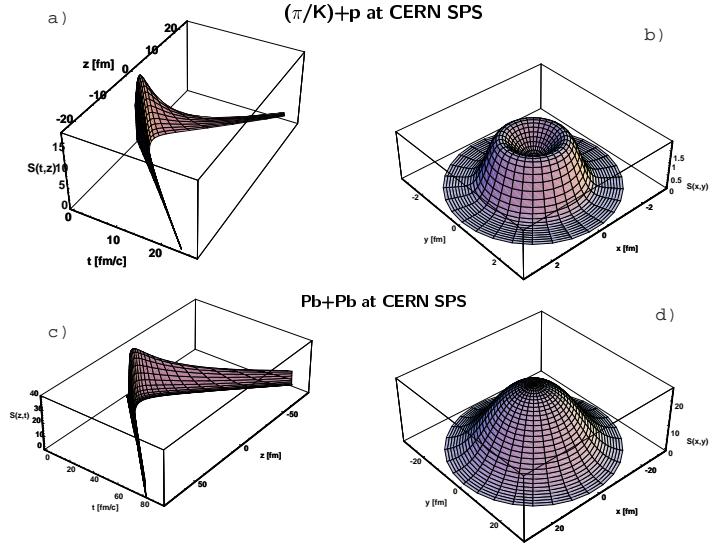


Fig. 25. The reconstructed emission function $S(t, z)$ in arbitrary vertical units, as a function of time t and longitudinal coordinate z (left diagrams), as well as the reconstructed emission function $S(x, y)$ in arbitrary vertical units, as a function of the transverse coordinates x and y (right pictures), for hh (upper pictures) and PbPb (lower pictures) collisions, respectively [78, 79, 80].

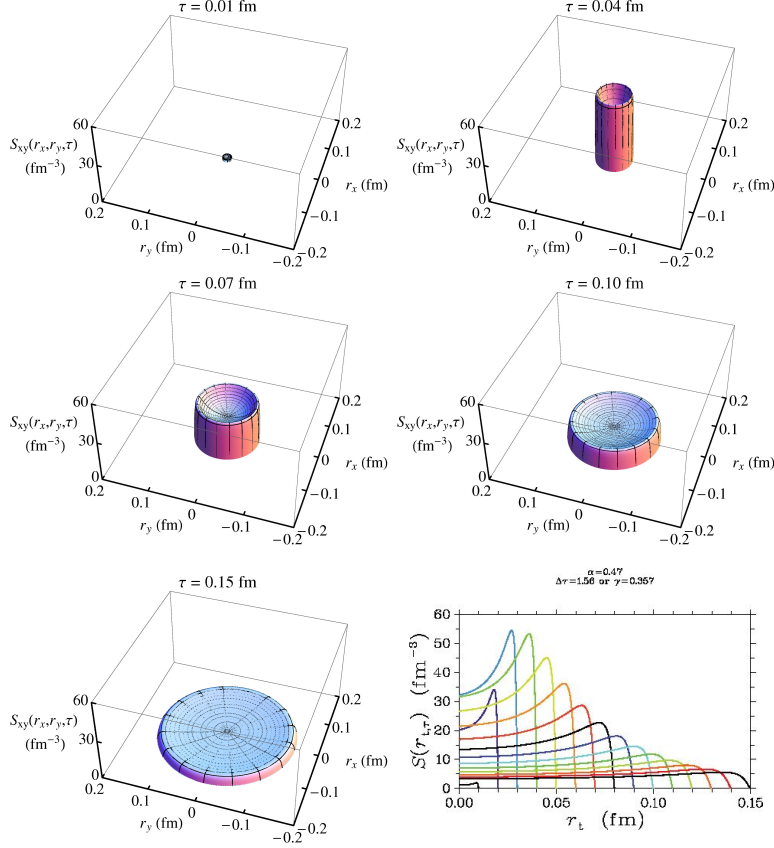


Fig. 26. The transverse emission function normalized to unity, and its transverse profile for various proper times [67]. An animated gif file covering the first 0.15 fm= 0.5×10^{-24} sec is available [82].

emission function for various proper times. Particle production starts immediately, increases rapidly and decreases slowly. In the transverse direction, a ring-like structure is observed similar to the expanding, ring-like wave created by a pebble in a pond. This ring like structure was also observed in hadron-hadron collisions [78] (Fig. 25 b)), where it was interpreted as due to the production of a fire-ring. Despite this similarity the physical process is different. Reflecting a non-thermal nature of e^+e^- annihilation, the proper-time distribution and space-time structure are reconstructed here without any reference to a temperature.

Interpolating and extrapolating Fig. 26, the proper-time dependence of the transverse expansion of the emission function can be best shown in a movie that ends in 0.15 fm (0.5×10^{-24} sec), making it the shortest movie

ever made of a process in nature [82].

In conclusion, I find it absolutely amazing how the combination of experimental results on single particle spectra and two-particle correlations with some theoretical interpretation can allow us to construct a "femtoscope" and actually watch particle production at a scale below one fm taking place in less than 10^{-24} sec !

However, one basic puzzle remains: why in the world should pions thought to be produced *coherently* in a flux tube (at least in e^+e^- and TeV pp collisions) be subject to *incoherent* Bose-Einstein correlations? Have we fooled ourselves for the past half century or more? Perhaps! What Todorova-Nová is trying to tell us in a series of papers [83] based on the Lund Helix model [84] is just that. Bose-Einstein correlations may not be needed to explain the charge asymmetry of pion pair production, a helix shaped flux tube would not only generate transverse momenta and hadronic masses, but a sharp correlation peak for like charged pion pairs at low values of four-momentum difference Q . I think, it should be a fruitful challenge for younger ones among us to help sort that out in detail in the future.

Acknowledgements. I would like to thank first of all Andrzej, himself, for almost half a century of direct and indirect encouragement and guidance in an attempt to understand multihadron dynamics, and I would like to thank Michal Praszalowicz and the organizers of this very special Symposium for the honor of being invited to contribute.

REFERENCES

- [1] L. Van Hove, *Phys. Lett.* **28B** (1969) 429 and *Nucl. Phys.* **B9** (1969) 331.
- [2] A. Białas, A. Eskreys, W. Kittel, S. Pokorski, J.K. Tuominiemi and L. Van Hove, *Nucl. Phys.* **B11** (1969) 479.
- [3] ABBCHLV Coll., J. Bertsch et al., *Nucl. Phys.* **B19** (1970) 381.
- [4] Chan Hong-Mo, J. Loskiewicz and W.W.M. Allison, *Nuovo Cim.* **57A** (1968) 93.
- [5] BDNPT Coll., G. Rinaudo et al., *Nucl. Phys.* **B25** (1971) 351.
- [6] J.E. Brau, F.T. Dao, M.F. Hodous, I.A. Pless and R.A. Singer, *Phys. Rev. Lett.* **27** (1971) 1481.
- [7] ABBC and ABBCW Coll., K. Bösebeck et al., *Nucl. Phys.* **B28** (1971) 381 and **B40** (1972) 39; ABBC and NPT Coll., J.V. Beaupré et al., *Nucl. Phys.* **B66** (1973) 93.
- [8] L. Van Hove, *Proc. IVth Int. Symp. on Multiparticle Hadrodynamics*, eds. A. Giovannini and S. Ratti, Pavia 1973.
- [9] ACNO Coll., J.J. Engelen et al., *Nucl. Phys.* **B167** (1980) 61.
- [10] B. Kahn, G.E. Uhlenbeck, *Physica* **5** (1938) 399.
- [11] K. Huang, *Statistical Mechanics*, John Wiley and Sons, 1963.
- [12] A.H. Mueller, *Phys. Rev.* **D4** (1971) 150.
- [13] M.G. Kendall and A. Stuart, *The Advanced Theory of Statistics*, Vol. 1, C. Griffin and Co., London 1969.
- [14] A. Białas and R. Peschanski, *Nucl. Phys.* **B273** (1986) 703; *ibid.* **B308** (1988) 857; A. Białas, *Multiparticle Dynamics*, Festschrift Van Hove, eds. A. Giovannini and W. Kittel (World Scientific, Singapore, 1990, p.75).
- [15] E.A. De Wolf, I.M. Dremin, W. Kittel, *Phys. Rep.* **270** (1996) 1.
- [16] JACEE Coll., T.H. Burnett et al., *Phys. Rev. Lett.* **50** (1983) 2062.
- [17] NA22 Coll., M. Adamus et al., *Phys. Lett.* **B185** (1987) 200.
- [18] Ya.B. Zeldovich, A.A. Ruzmaikin, D.D. Sokoloff in *The Almighty Chance*, World Scientific Lecture Notes in Physics, Vol. 20 (World Scientific, Singapore, 1990).
- [19] G. Bédard, *Proc. Phys. Soc.* **90** (1967) 131; D. Cantrell, *Phys. Rev.* **A1** (1970) 672.
- [20] W. Kittel and E.A. De Wolf, *Soft Multihadron Dynamics*, World Scientific (2005).
- [21] P. Lipa and B. Buschbeck, *Phys. Lett.* **B223** (1989) 465; R. Hwa, *Phys. Rev.* **D41** (1990) 1456.
- [22] A. Białas, *Nucl. Phys.* **A525** (1991) 345c.
- [23] E.K.G. Sarkisyan, *Phys. Lett.* **B477** (2000) 1; I.G. Abbiendi et al. (OPAL), *Phys. Lett.* **523** (2001) 35.
- [24] W. Ochs and J. Wośiek, *Phys. Lett.* **B214** (1988) 617; **B232** (1989) 271.

- [25] NA22 Coll., I.V. Ajinenko et al., *Phys. Lett.* **B197** (1987) 457.
- [26] L. Van Hove, *Ann. Phys.* **192** (1989) 66.
- [27] A. Białas et al., *Phys. Lett.* **B229** (1989) 398.
- [28] N.M. Agababyan et al. (NA22), *Phys. Lett.* **B261** (1991) 165.
- [29] C. Albajar et al. (UA1), *Nucl. Phys.* **B345** (1990) 1; B. Buschbeck, *Festschrift L. Van Hove*, eds. A. Giovannini and W. Kittel (World Scientific, Singapore, 1990) p. 211; P. Lipa, Ph.D. Thesis, Univ. of Vienna 1990; P. Lipa et al., *Proc. Ringberg Workshop on Multiparticle Production*, Ringberg Castle, Germany 1991, eds. R.C. Hwa, W. Ochs and N. Schmitz (World Scientific, Singapore, 1992) p. 111; N. Neumeister et al., *Z. Phys.* **C60** (1993) 633; *Acta Phys. Slovaca* **44** (1994) 113.
- [30] A. Capella, K. Fialkowski and A. Krzywicki, *Phys. Lett.* **230B** (1989) 149.
- [31] A. Białas, *Festschrift L. Van Hove*, eds. A. Giovannini and W. Kittel (World Scientific, Singapore, 1990) p. 75.
- [32] D. Seibert, *Phys. Lett.* **B240** (1990) 215.
- [33] M.I. Adamovich et al. (EMU-01), *Phys. Rev. Lett.* **65** (1990) 412; *Phys. Lett.* **B263** (1991) 539; *Z. Phys.* **C49** (1991) 395; *Nucl. Phys.* **B388** (1992) 3; *Phys. Lett.* **B407** (1997) 92.
- [34] B. Wosiek et al. (KLMM), *Proc. XXVth Int. Symp. on Multiparticle Dynamics*, Stara Lesná 1995, eds. D. Bruncko, L. Šándor and J. Urbán (World Scientific, Singapore, 1996) p.271.
- [35] L. Verluyten et al. (WA59 and E180), *Phys. Lett.* **B260** (1991) 456.
- [36] T. Åkesson et al. (HELIOS), *Phys. Lett.* **B252** (1990) 303.
- [37] H.G.E. Hentschel and I. Procaccia, *Physica* **8D** (1983) 435; P. Grassberger, *Phys. Lett.* **97A** (1983) 227.
- [38] N. Agababyan et al. (NA22), *Z. Phys.* **C59** (1993) 405; M. Charlet, PhD Thesis, Nijmegen, 1994.
- [39] P. Carruthers and I. Sarcevic, *Phys. Rev. Lett.* **63** (1989) 1562.
- [40] H.C. Eggers et al., *Phys. Rev.* **D48** (1993) 2040; M. Charlet, *Proc. XXIIIrd Int. Symp. on Multiparticle Dynamics*, Aspen 1993, eds. M.M. Block and A.R. White (World Scientific, Singapore, 1994) p.302.
- [41] F. Mandl and B. Buschbeck in *Proc. Cracow Workshop on Multiparticle Production*, eds. A. Białas et al. (World Scientific, Singapore, 1994) p.1.
- [42] N.M. Agababyan et al. (NA22), *Phys. Lett.* **B332** (1994) 458.
- [43] M.R. Adams et al. (E665), *Phys. Lett.* **B335** (1994) 535.
- [44] A. Białas, *Nucl. Phys.* **A545** (1992) 285; A. Białas, *Acta Phys. Pol.* **B23** (1992) 561.
- [45] P. Bak, C. Tang and K. Wiesenfeld, *Phys. Rev. Lett.* **59** (1987) 381; P. Bak and K. Chen, *Scientific American* **264** (1991) 46.
- [46] W. Kittel, *Acta Phys. Pol.* **B32** (2001) 3927.
- [47] G. Alexander, *Rep. Prog. Phys.* **66** (2003) 481.

- [48] S.V. Akkelin, Yu.M. Sinyukov, *Phys. Lett.* **B356** (1995) 521; *Z. Phys.* **C72** (1996) 501.
- [49] NA22 Coll., N.M. Agababyan et al., *Z. Phys.* **C71** (1996) 405.
- [50] L3 Coll., M. Acciari et al., *Phys. Lett.* **B458** (1999) 517; DELPHI Coll., P. Abreu et al., *Phys. Lett.* **B471** (2000) 460; OPAL Coll., G. Abbiendi et al., *Z. Phys.* **C16** (2000) 423; ALEPH Coll., A. Heister et al., CERN-EP/2003-079.
- [51] ZEUS Coll., S. Chekanov et al., *Phys. Lett.* **B583** (2004) 231.
- [52] STAR Coll. C. Adler et al., *Phys. Rev. Lett.* **87** (2001) 082301; J. Adams et al., nucl-ex/0312009.
- [53] NA22 Coll., N.M. Agababyan et al., *Phys. Lett.* **B422** (1998) 359; A. Ster, T. Csörgő, B. Lörstad, *Nucl. Phys.* **A661** (1999) 419; M. Csanád, T. Csörgő, B. Lörstad, A. Ster, *Acta Phys. Pol.* **B35** (2004) 191; nucl-th/0402037; hep-ph/0406042.
- [54] T. Csörgő, S. Hegyi, W.A. Zajc, *Eur. Phys. J.* **C36** (2004) 67.
- [55] NA44 Coll., H. Beker et al., *Z. Phys.* **C64** (1994) 209; I.G. Bearden et al., *Phys. Rev. Lett.* **87** (2001) 112301; NA49 Coll., S.V. Afanasiev et al., *Phys. Lett.* **B557** (2003) 157.
- [56] PHENIX Coll., J. Adcox et al., *Phys. Rev. Lett.* **88** (2002) 192302; S.S. Adler et al., nucl-ex/0401003; PHOBOS Coll., B.B. Back et al., nucl-ex/0406027.
- [57] B. Lörstad, O.G. Smirnova, Proc. 7th Int. Workshop on Multiparticle Production, eds. R.C. Hwa et al. (World Scientific, Singapore, 1997) p.42.
- [58] T. Csörgő and J. Zimányi, *Nucl. Phys.* **A517** (1990) 588; A. Białas and K. Zalewski, *Acta Phys. Pol.* **B30** (1999) 359.
- [59] NA22 Coll., N.M. Agababyan et al., *Z. Phys.* **C68** (1995) 229.
- [60] L3 Coll., P. Achard et al., *Phys. Lett.* **B540** (2002) 185.
- [61] NA44 Coll., H. Bøggild et al., *Phys. Lett.* **B455** (1999) 77; I.G. Bearden et al., *Phys. Lett.* **B517** (2001) 25.
- [62] WA98 Coll., N.N. Aggarwal et al., *Phys. Rev. Lett.* **85** (2000) 2895.
- [63] STAR Coll., J. Adams et al., *Phys. Rev. Lett.* **91** (2003) 262301.
- [64] M.A. Braun, F. del Moral and C. Pajares, *Phys. Lett.* **B551** (2003) 291.
- [65] E877 Coll., D. Miskowiec et al., *Nucl. Phys.* **A590** (1995) 473c; E895 Coll., M.A. Lisa et al., *Phys. Lett.* **B496** (2000) 1.
- [66] STAR Coll., J. Adams et al., *Phys. Rev. Lett.* **93** (2004) 012301.
- [67] L3 Coll., P. Achard et al., *Eur. Phys. J.* **C71** (2011) 1648; T. Novák, PhD Thesis, Nijmegen (2008).
- [68] CMS Coll., V. Khachatryan et al., *JHEP* **1105** (2011) 029.
- [69] ATLAS Coll., Róbert Astaloš, PhD thesis, 2015, Nijmegen and Bratislava; W.J. Metzger, The τ -model of Bose-Einstein Correlations: Some recent results, arXiv:1512.04301
- [70] T. Csörgő and J. Zimányi, *Nucl. Phys.* **A517** (1990) 588.
- [71] A. Białas and K. Zalewski, *Acta Phys. Pol.* **B30** (1999) 359; A. Białas et al., *Phys. Rev.* **D62** (2000) 114007.

- [72] T. Csörgő, W. Kittel, W.J. Metzger and T. Novák, *Phys. Lett.* **B663** (2008) 214 and W.J. Metzger, T. Novák, W. Kittel and T. Csörgő, *Int. J. Mod. Phys.* **E16** (2008) 3224.
- [73] P. Dahlqvist, B. Andersson and G. Gustafson, *Nucl. Phys.* **B328** (1989) 76; G. Gustafson and A. Nilsson, *Nucl. Phys.* **B355** (1991) 106; G. Gustafson and A. Nilsson, *Z. Phys.* **C52** (1991) 533.
- [74] R. Metzler, J. Klafter, *Phys. Rep.* **339** (2000) 1.
- [75] T. Csörgő, S. Hegyi and W.A. Zajc, *Eur. Phys. J.* **C36** (2004) 67.
- [76] J. P. Nolan, *Stable Distributions - Models for Heavy Tailed Data*, (Birkhäuser, Boston, 2010), In progress, Chapter 1 online at academic2.american.edu/~jp-nolan.
- [77] A. Białas and K. Zalewski, *Phys. Lett.* **B727** (2013) 182; A. Białas, W. Florkowski and K. Zalewski, *Phys. Lett.* **B748** (2015) 9.
- [78] NA22 Coll., N.M. Agababyan et al., *Phys. Lett.* **B422** (1998) 359.
- [79] A. Ster and T. Csörgő, *AIP Conference Proc.* **828** (2006) 572.
- [80] A. Ster, T. Csörgő and B. Lörsstad, *Nucl. Phys.* **A661** (1999) 419.
- [81] T. Csörgő, *Simple Analytic Solution of Fireball Hydrodynamics*, nucl-th/9809011.
- [82] T. Novák, T. Csörgő, www.kfki.hu/~csorgo/L3/plots/movie.gif and www.kfki.hu/~csorgo/L3/plots/Sxyt.gif
- [83] Š. Todorova-Nová, *Phys. Rev.* **D89** (2014) 015002; *Phys. Rev.* **D86** (2012) 034001; *Quantum Properties of QCD String Fragmentation*, XLV Int. Symp. on Multiparticle Dynamics, Wildbad Kreuth, 2015.
- [84] B. Andersson, G. Gustafson, J. Hakkinen, M. Ringner and P. Sutton, *JHEP* **9809** (1998) 014.